catalysts

MDPI

Article

Ni-H-Beta Catalysts for Ethylene Oligomerization: Impact of Parent Cation on Ni Loading, Speciation, and Siting

Joseph McCaig and H. Henry Lamb *

Department of Chemical and Biomolecular Engineering, North Carolina State University, Raleigh, NC 27695, USA; jmccaig@ncsu.edu
* Correspondence: lamb@ncsu.edu

Abstract: Ni-H-Beta catalysts for ethylene oligomerization (EO) were prepared by ion exchange of NH_4-Beta and H-Beta zeolites with aqueous $Ni(NO_3)_2$ and characterized by H_2-temperature-programmed reduction (TPR), NH_3-temperature-programmed desorption (TPD), and diffuse-reflectance infrared Fourier-transform spectroscopy (DRIFTS). Quadruple exchange of NH_4-Beta at 70 °C resulted in 2.5 wt.% Ni loading corresponding to a Ni^{2+}/framework aluminum (FAl) molar ratio of 0.52. $[NiOH]^+$ and H^+ are the primary charge-compensating cations in the uncalcined catalyst, as evidenced by TPR and DRIFTS. Subsequent calcination at 550 °C in air yielded a Ni-H-Beta catalyst containing primarily bare Ni^{2+} ions bonded to framework oxygens. Quadruple exchange of H-Beta at 70 °C gave 2.0 wt.% Ni loading (Ni^{2+}/FAl = 0.41). After calcination at 550 °C, the resulting Ni-H-Beta catalyst comprises a mixture of bare Ni^{2+} ions: $[NiOH]^+$ and NiO species. The relative abundance of $[NiOH]^+$ increases with the number of exchanges. In situ pretreatment at 500 °C in flowing He converted the $[NiOH]^+$ species to bare Ni^{2+} ions via dehydration. The bare Ni^{2+} ions interact strongly with the Beta framework as evidenced by a perturbed antisymmetric T-O-T vibration at 945 cm^{-1}. DRIFT spectra of CO adsorbed at 20 °C indicate that the Ni^{2+} ions occupy two distinct exchange positions. The results of EO testing at 225 °C and 11 bar (ethylene) suggested that the specific Ni^{2+} species initially presented (e.g., bare Ni^{2+}, $[NiOH]^+$) did not significantly affect the catalytic performance.

Keywords: Bronsted acidity; TPR; DRIFTS; NH_3 TPD; perturbed TOT skeletal vibration; CO adsorption

Citation: McCaig, J.; Lamb, H.H. Ni-H-Beta Catalysts for Ethylene Oligomerization: Impact of Parent Cation on Ni Loading, Speciation, and Siting. *Catalysts* **2022**, *12*, 824. https://doi.org/10.3390/catal12080824

Academic Editors: Yuanhua Sang and Zupeng Chen

Received: 15 June 2022
Accepted: 19 July 2022
Published: 27 July 2022

1. Introduction

Approximately 150 billion cubic meters of natural gas are flared in the United States each year, releasing CO_2 into the atmosphere. Often, this waste is the result of geographic isolation; existing pipeline infrastructure is aging and ill-equipped to service new sources of natural gas, such as those derived from shale oil production [1,2]. Recently, a modular gas-to-liquid technology has been proposed, whereby "stranded" natural gas liquids (NGLs) are converted to olefinic liquid fuels at the site of production. Relative to the costly and energy-intensive transportation of gases by pipeline, liquids can be transported off site economically by tanker or truck [3]. In the proposed scheme, following the conversion of ethane to ethylene via cyclic redox oxidative dehydrogenation [4], ethylene is converted to liquid C4-C12 oligomers over heterogeneous Ni catalysts.

For many years, ethylene oligomerization (EO) has been practiced industrially using Ni-based homogeneous catalysts to produce feedstocks for surfactants, lubricants, and plasticizers [5]. Numerous processes have been developed and patented by the major oil and gas producers (Shell Higher Olefin process, Chevron Gulf process) [6]. Because of the significant environmental drawbacks of homogenous catalysis (e.g., catalyst separation and recovery), research has focused on heterogeneous EO. Catalysts comprising Ni supported on aluminosilicates have received attention because of their excellent catalytic performance under mild conditions, low cost, and easy preparation. Although zeolite Y, amorphous SiO_2-Al_2O_3 (ASA), AlSBA-15, Siral-30, and AlMCM-41 have been employed successfully

as catalyst supports [7–12], the work presented herein focuses on Ni^{2+}-exchanged zeolite Beta. Zeolite Beta has a three-dimensional micropore network comprising 12-membered rings with ~0.7 nm free apertures. Moreover, the commercial zeolite Beta employed in this work has a hierarchical mesoporosity that effectively reduces the impact of mass-transfer limitations [13].

Ni-H-Beta catalysts for EO were first reported by Martinez et al. [13], and subsequent research has aimed to elucidate the nature of the active sites [14–19]. Ni-H-Beta has been the subject of experimental and theoretical investigations over the past decade, seeking to identify the EO-active sites, calculate kinetic parameters, establish reaction mechanisms, and quantify the impact of Ni^{2+}/H^+ ratios on product distribution. Briefly, Ni^{2+} ions in exchange positions have been identified as the precursors of Cossee–Arlman active centers that perform oligomerization via a coordination–insertion mechanism. The Ni-catalyzed oligomerization reaction produces even-numbered linear α-olefins (ELAO) with a Schulz–Flory statistical distribution. Bronsted acid sites (BAS) perform co-oligomerization, cracking, and branching isomerization; the Ni^{2+}/H^+ ratio determines the distribution of ELAO, branched, and odd-numbered oligomers.

This work assesses the impact of parent cation (H^+, NH_4^+) on Ni loading, speciation, and siting in Ni-H-Beta catalysts prepared by aqueous ion exchange. Catalysts were characterized by H_2-temperature-programmed reduction (TPR), NH_3-temperature-programmed desorption (TPD), and diffuse-reflectance Fourier-transform infrared spectroscopy (DRIFTS) before and after CO adsorption at 20 °C. The catalysts were tested for EO conversion and selectivity at 225 °C and 11 bar using a fixed-bed microreactor equipped for online gas chromatography (GC) analysis.

2. Results and Discussion

2.1. Catalyst Preparation

The XRD patterns of the parent zeolites and selected Ni-H-Beta (H^+-*n*x) catalysts (Figure S1, Supplementary Materials) are fully consistent with the polymorphic crystal structures of zeolite Beta, and the absence of diffraction peaks from other phases (e.g., NiO) suggests high dispersion of the supported Ni^{2+} species. The Ni loadings and BET surface areas of the catalysts are given in Table 1. The BET surface areas of the Ni-containing catalysts are generally equivalent to or slightly lower than that of the parent NH_4-Beta and H-Beta zeolites (640 and 622 m^2/g, respectively). The Ni-NH_4-Beta catalyst has a lower BET surface area, but this catalyst was not calcined after ion exchange. The total pore volumes of NH_4-Beta and H-Beta (0.81 and 0.74 cm^3/g, respectively) are indicative of significant mesoporosity. BJH pore–size distributions of the parent zeolites and selected Ni-containing catalysts (Figure S2, Supplementary Materials) reveal 3.8, 7, and 35 nm mesopores. The total pore volumes of the Ni-containing catalysts are in the 0.66–0.88 cm^3/g range, and the BJH pore–size distributions are similar to those of the parent zeolites.

Table 1. Properties of Ni-H-Beta catalysts.

Catalyst [a]	Ni (wt.%)	S_{BET} (m^2/g)	Ni/FAl Molar Ratio [b]	TPR H/Ni Ratio		NH_3/Ni Ratio [d]	H_2/N_2 Ratio [d]
				300 °C [c]	500 °C [c]		
Ni-H-Beta (H^+-4x)	2.02	620	0.41	1.56	1.56	n/a	n/a
Ni-H-Beta (H^+-3x)	2.14	n/a	0.44	1.50	1.43	0.43	2.0
Ni-H-Beta (H^+-2x)	1.98	610	0.40	1.43	1.45	0.71	-
Ni-H-Beta (H^+-1x)	1.17	n/a	0.24	1.31	n/a	0.84	-
Ni-H-Beta (NH_4^+-4x)	2.64	602	0.54	1.98	n/a	0.44	2.6
Ni-NH_4-Beta [e]	2.54	560	0.52	2.21	1.75	0.80	2.1

[a] Consult Section 3 for nomenclature; [b] based on NH_4^+-exchange capacity from TPDE; [c] in situ pretreatment temperature; [d] calculated from 550 °C peak in NH_3 TPD spectrum; [e] prepared by quadruple exchange of NH_4-Beta.

The temperature-programmed decomposition (TPDE) spectrum of NH_4-Beta (Figure 1A) exhibits a very broad NH_3 evolution peak at ~400 °C, resulting from the decomposition of NH_4^+ ions associated with FAl sites to H^+ and molecular NH_3. Very small amounts of H_2 and N_2 also evolved around 520 °C. Using the NH_3 peak area, the FAl concentration (monovalent exchange capacity) for NH_4-Beta was estimated at 0.85 mmol/g. This value is significantly less than the ~1.4 mmol/g based on the overall composition (using the Si/Al ratio provided by the manufacturer). We attribute this difference to extra-framework aluminum (EFAl), as evidenced by DRIFTS (*vide infra*) [20]. Catalysts prepared from NH_4-Beta exhibit Ni loadings of ~2.6 wt.% after quadruple exchange. Because each bare Ni^{2+} ion can compensate the charge of two proximate framework aluminum (FAl) ions (FAl pairs), a maximum Ni/FAl ratio of 0.5 is expected [21]. Based on the measured FAl concentration, the Ni/FAl ratio for Ni-NH_4-Beta (Table 1) corresponds to 104% exchange or 4% "over-exchange". Because FAl is not present as proximate pairs, this high degree of exchange suggests the involvement of monovalent ions, e.g., $[NiOH]^+$. Interestingly, the TPDE spectrum of Ni-NH_4-Beta (Figure 1B) does not show NH_3 evolution, but there are well-defined peaks at 400 and ~550 °C arising from concomitant H_2 and N_2 evolution. These products are consistent with NH_3 decomposition; however, the H/N ratio is ~2 rather than the expected 3. The TPDE results suggest the absence of intrazeolitic NH_4^+ ions and that instead NH_3 molecules coordinate Ni^{2+} ions following ion exchange of NH_4-Beta. This is plausible because of reversible decomposition of NH_4^+ ions to NH_3 and H^+ in aqueous solution. Calcination of Ni-NH_4-Beta at 550 °C in air yields Ni-H-Beta (NH_4^+-4x). The slightly higher measured Ni loading of this catalyst corresponds to ~8% over-exchange.

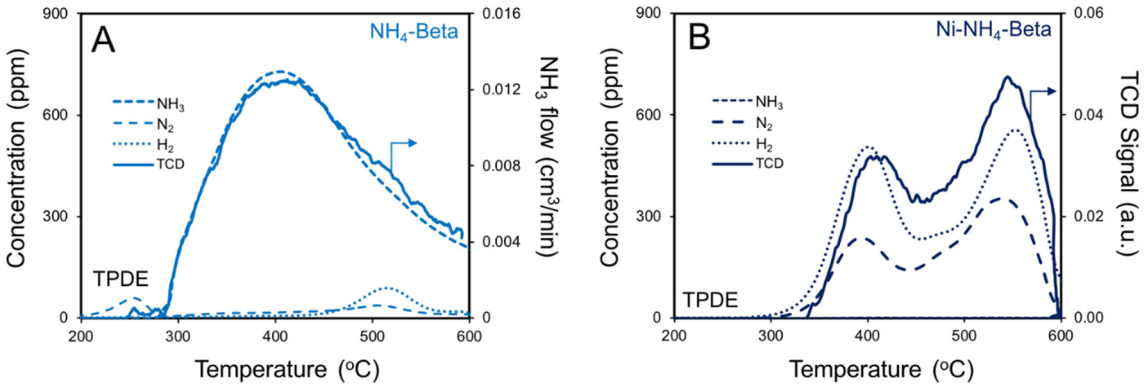

Figure 1. TPDE spectra. (**A**) NH_4-Beta and (**B**) Ni-NH_4-Beta after in situ pretreatment at 300 °C.

For catalysts prepared from H-Beta, Ni loading increased approximately twofold between the first and second exchanges; however, subsequent exchanges did not result in significant loading increases. The Ni loadings are ~2 wt.% after two to four exchanges. The maximum loading (observed for Ni-H-Beta (H^+-3x)) corresponded to ~88% exchange. Partial hydrolysis of FAl sites in aqueous media provides a plausible explanation for the lower maximum loading of catalysts prepared from H-Beta. FAl species in hydrogen zeolites (especially those in proximal pairs) are converted via Si-O-Al bond hydrolysis from tetrahedral to octahedral coordination when exposed to aqueous media (see scheme in Figure 2) [22–24]. Conversely, if the charge-compensating cation is Na^+ or NH_4^+, FAl species are stable in aqueous media [22]. For zeolite Beta, it has been observed that one of the two crystallographically distinct T-sites occupied by Al^{3+} is selectively hydrolyzed to form an octahedral cation [25]. The Al^{3+} ion is coordinated by 2 H_2O molecules, 3 framework oxygens, and a OH^- group which contains the H^+ that originally occupied the exchange position [26]. Thus, this proton is no longer available for ion exchange with Ni^{2+}, thereby reducing the overall exchange capacity. The resultant octahedral Al^{3+} species is termed "framework associated"; this process is reported to be fully reversible upon dehydration at high temperatures (e.g., 500 °C). For Beta with Si/Al = 12.5, up to 25% of such sites may be hydrolyzed [24]. Because the Ni loading is approximately 20% lower in the case of H-Beta

exchange, we infer that pairs of Al-containing T-sites are hydrolyzed; otherwise, the drop in Ni uptake would be greater.

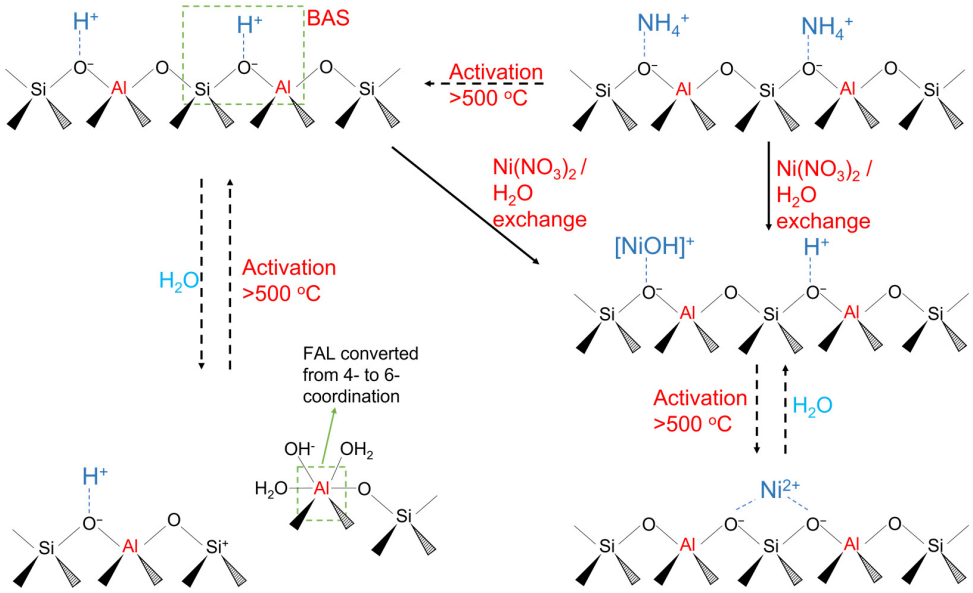

Figure 2. Scheme illustrating the parent cation-dependent aqueous ion-exchange chemistry of Ni^{2+} species in zeolite Beta.

2.2. H_2 TPR

TPR profiles of the Ni-H-Beta catalysts prepared from H-Beta are shown in Figure 3A. The profiles of Ni-H-Beta (H^+-*n*x), *n* = 3, 4 after in situ pretreatment (dehydration) at 300 °C contain three reduction features: a low-temperature peak (or shoulder) at ~350 °C, a sharp peak at ~450 °C, and a relatively large broad peak at ~600 °C. The high-temperature peak is assigned to reduction of bare Ni^{2+} ions in exchange positions based on extensive literature [27–31]. Increasing the pretreatment temperature to 500 °C results in the elimination of the 450 °C peak with a concomitant increase in the high-temperature peak area. For Ni-H-Beta (H^+-3x), the Ni^{2+} peak narrows and shifts from 600 to 580 °C. The low-temperature TPR peak is now clearly resolved and can be assigned to NiO [30,31]. The sharp TPR peak at 450 °C may be assigned to $[NiOH]^+$ moieties with an adjacent BAS. Such proximal $[NiOH]^+/H^+$ pairs were originally proposed by Ward to explain the Bronsted acidity of zeolite Y exchanged with divalent cations [32]. We infer that the $[NiOH]^+/H^+$ pairs dehydrate during 500 °C pretreatment yielding bare Ni^{2+} ions in exchange positions (see scheme in Figure 2). Previously, NiO has been suggested to form via a parallel pathway involving the dehydration of $[NiOH]^+$ and an adjacent BAS [32]. The TPR profile of Ni-H-Beta (H^+-2x) after activation at 300 °C contains a strong peak at ~530 °C and a small one at 350 °C that are assigned to reduction of Ni^{2+} ions in exchange positions and NiO, respectively. Although Ni-H-Beta (H^+-2x) does not exhibit a sharp peak at 450 °C, the main TPR peak is asymmetric with a shoulder at this temperature. Increasing the activation temperature to 500 °C eliminates the asymmetry and results in a much narrower peak at ~560 °C. A NiO reduction peak at 350 °C is clearly resolved. The formation of $[NiOH]^+$ species appears to be most prevalent for catalysts subjected to 3–4 exchange cycles, indicating that the extent of Ni^{2+} ion hydrolysis increases with the number of exchanges [33]. The TPR profile of Ni-H-Beta (H^+-1x) after in situ pretreatment at 300 °C shows only small features at 350 °C and 400 °C corresponding to the reduction of NiO and $[NiOH]^+$species, respectively. The typical peak at ~600 °C for reduction of Ni^{2+} ions in exchange positions is not observed; however, the TCD signal begins to rise at ~500 °C, and the detector does not return to baseline at 800 °C.

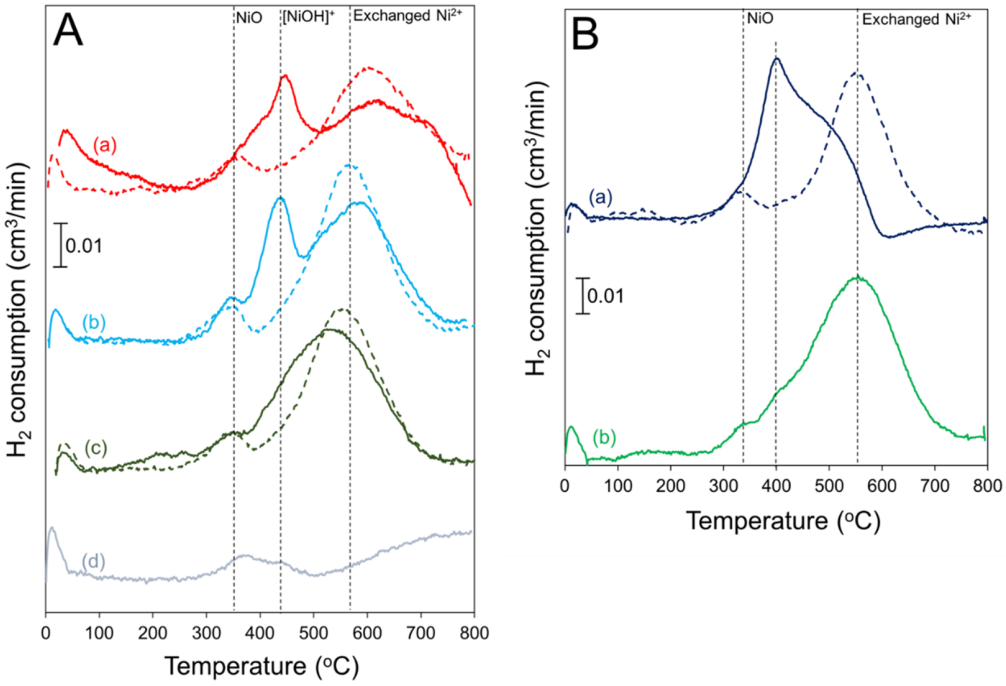

Figure 3. H_2 TPR profiles of catalysts after in situ pretreatment at 300 °C (solid lines) and 500 °C (dashed lines). (**A**) (a) Ni-H-Beta (H^+-4x), (b) (H^+-3x), (c) (H^+-2x), (d) (H^+-1x); (**B**) (a) Ni-NH_4-Beta, (b) Ni-H-Beta ($NH_4{}^+$-4x).

The TPR profiles of catalysts derived from NH_4-Beta are shown in Figure 3B. After pretreatment at 300 °C, Ni-NH4-Beta exhibits an intense peak at 400 °C with a shoulder at ~500 °C and a small negative peak at 600 °C. As evidenced by online QMS (see Figure S3, Supplementary Materials), the negative peak at 600 °C results from NH_3 decomposition to H_2 and N_2 and coincides with the second TPDE peak noted above. The sharp peak at 400 °C is assigned to $[NiOH]^+$ species analogous to those identified in the Ni-H-Beta (H^+-*n*x), n = 3, 4 catalysts. We infer from the TPR profile of Ni-NH_4-Beta after in situ pretreatment at 500 °C that the $[NiOH]^+$ species have been dehydrated yielding bare Ni^{2+} ions, balancing the FAl pairs. The TPR profile of Ni-H-Beta ($NH_4{}^+$-4x) consists of a broad reduction peak centered at 550 °C assigned to bare Ni^{2+} ions in exchange positions, a shoulder at 400 °C assigned to $[NiOH]^+$, and a small band at 360 °C assigned to NiO. We infer that Ni^{2+} ions exchange in NH_4-Beta as $[NiOH]^+/H^+$ pairs which are converted to bare Ni^{2+} ions upon calcination at 550 °C in air or pretreatment in an inert ambient at 500 °C (see scheme in Figure 2).

The TPR H/Ni ratios (Table 1) for the Ni-H-Beta (H^+-*n*x) catalysts are significantly less than expected for reduction of Ni^{2+} to Ni^0, and the deficit is greatest for Ni-H-Beta (H^+-1x). In contrast, the TPR of Ni-H-Beta ($NH_4{}^+$-4x) yields a H/Ni ratio of 2. With the exception of Ni-H-Beta (H^+-1x): (i) the TCD signals return to baseline (or very nearly so) before the temperature reaches 800 °C, suggesting complete reduction; (ii) the H/Ni ratios are equivalent after pretreatment at 300 and 500 °C, which is consistent with dehydration without a change in oxidation state; (iii) the H/Ni ratios increase modestly with the number of exchanges. Formation of intrazeolitic Ni^{2+} species that reduce only at >800 °C could explain the lower-than-expected H/Ni ratio and the absence of the expected peak from reduction of Ni^{2+} ions in exchange positions for Ni-H-Beta (H^+-1x). Ni species that require unusually high reduction temperatures have been reported in Ni-ZSM-5 catalysts prepared by impregnation [30,34]. Alternatively, the autoreduction in Ni^{2+} ions in zeolite Beta has been suggested to explain the lower-than-expected H/Ni ratios [31]:

$$BEA^-[NiOH]^+ \rightarrow Ni^0 + HBEA + \frac{1}{2}O_2$$

The H/Ni ratio for Ni-NH_4-Beta after pretreatment at 300 °C is slightly greater than 2 because of co-reduction of adventitious carbon species, as evidenced by concomitant CH_4 evolution (Figure S3, Supplementary Materials). In contrast, the H/Ni ratio for Ni-NH_4-Beta after pretreatment at 500 °C is somewhat less than 2. In this case, H_2 produced during thermal activation at 500 °C may reduce some Ni^{2+} species, resulting in a lower H/Ni ratio.

2.3. DRIFTS

The DRIFT spectrum (Figure 4A) of H-Beta in the O-H stretching (υ_{OH}) region contains a band at 3607 cm^{-1}, which is characteristic of bridging Si-OH-Al moieties (isolated BAS); the bands at 3746 and 3665 cm^{-1} are assigned to external silanol groups and EFAl species, respectively [35]. Internal silanol groups (3732 cm^{-1}), although present after calcination of H-Beta at 500 °C, are effectively eliminated by calcination at 600 °C (see Figure S4). Internal silanol groups are associated with structural defects, such as Al^{3+} vacancies resulting from dealumination or stacking faults in the Beta structure [35,36]. EFAl species comprise Al^{3+} ions that have been completely and irreversibly removed from the framework, and a number of coordination environments (including 3 OH^- groups and 3 H_2O molecules) have been proposed [37,38]. EFAl properties are dependent on the parent zeolite and method of dealumination [37,39], and some researchers have inferred that EFAl species exhibit Lewis acidity [40]. In addition, a very high frequency (VHF) band at 3782 cm^{-1} is observed. Typically, this band is attributed to tri-coordinated-framework-associated Al species (SiO-Al(OH)-OSi) which form via bridging Si-(OH)-Al groups upon calcination [41].

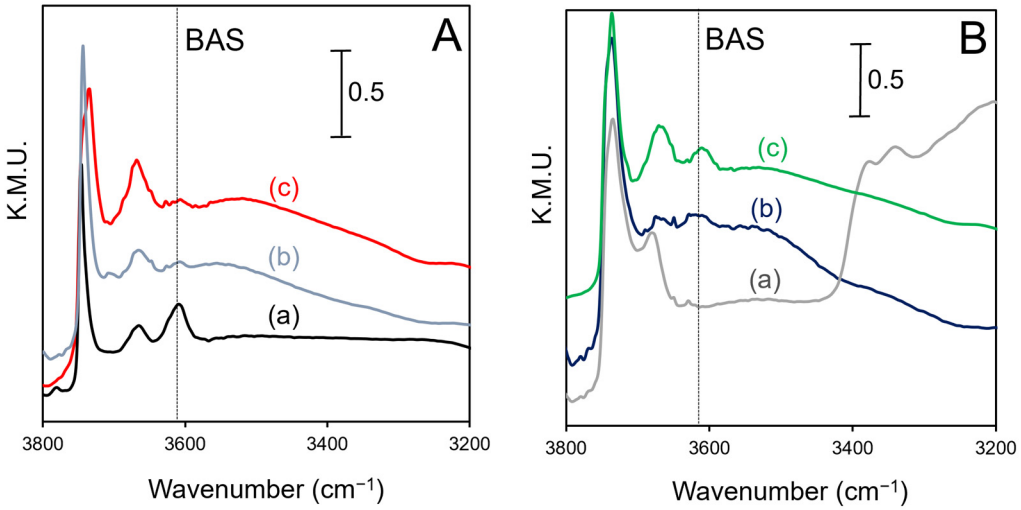

Figure 4. DRIFT spectra in the υ_{OH} region of catalysts after in situ pretreatment at 350 °C. (**A**) (a) H-Beta, (b) Ni-H-Beta (H^+-1x), (c) Ni-H-Beta (H^+-4x); (**B**) (a) NH_4-Beta, (b) Ni-NH_4-Beta, (c) Ni-H-Beta (NH_4^+-4x).

The υ_{OH} DRIFT spectra (Figure 4A) of Ni-H-Beta (H^+-*n*x), *n* = 1, 4 are similar to that of H-Beta; however, the small VHF band has disappeared, and the internal silanol and EFAl bands are much more prominent. As expected, the isolated BAS bands decrease in intensity following Ni^{2+} exchange. If each Ni^{2+} cation replaced 2 H^+, the isolated BAS peak should be nearly eliminated in Ni-H-Beta (H^+-4x), and it is greatly diminished. The Ni-H-Beta (H^+-*n*x), *n* = 1, 4 catalysts also exhibit a broad band centered at 3550 cm^{-1} that is attributed to perturbed (H-bonded) bridging OH groups [42], and this band appears to increase in intensity after Ni^{2+} exchange. The TPR results indicate that $[NiOH]^+$ species are abundant in Ni-H-Beta (H^+-4x) after activation at 300 °C; however, a υ_{OH} band corresponding to $[NiOH]^+$ species was not identified. Overlap with the EFAl band is possible based on the literature data for $Ni(OH)_2$ and $[CuOH]^+$ in SSZ-13 [43,44], and the EFAl band of Ni-H-Beta (H^+-4x) is substantially larger than that of Ni-H-Beta (H^+-1x).

The υ_{OH} DRIFT spectrum of NH_4-Beta (Figure 4B) contains bands at 3745 and 3665 cm^{-1} that are assigned to external silanol groups and EFAl species, respectively, and strong N-H stretching bands in the 3200–3400 cm^{-1} region. In contrast, N-H stretching bands are barely detectable in the DRIFT spectrum of Ni-NH_4-Beta, indicating nearly complete loss of NH_4^+ ions during ion exchange. Small EFAl and BAS peaks are visible, but these bands are poorly resolved because of residual water on the dried catalyst after in situ pretreatment at 350 °C. The detection of BAS in Ni-NH_4-Beta is consistent with hydrolysis of aqueous Ni^{2+} ions resulting in $[NiOH]^+/H^+$ pairs, as inferred based on TPR. Subsequent calcination of Ni-NH_4-Beta at 550 °C in air yields Ni-H-Beta (NH_4^+-4x), which has a υ_{OH} spectrum similar to H-Beta albeit with a much stronger EFAl band. Interestingly, the bridging OH (BAS) band of Ni-H-Beta (NH_4^+-4x) is more intense than that of the Ni-H-Beta (H^+-*n*x) catalysts, but the presence of H-bonded BAS may affect the magnitude of the 3607 cm^{-1} band.

DRIFT spectra of H-Beta, NH_4-Beta, and the Ni-H-Beta catalysts in the T-O-T "transmission window" (900–1000 cm^{-1}) are shown in Figure 5. Small features between 950 and 1000 cm^{-1} are observed for the parent zeolites that likely arise from transition metal ion impurities. New peaks are observed for the Ni-H-Beta catalysts that evidence strong interaction of Ni^{2+} ions with the zeolite framework. Previously, similar evidence for interaction of "bare" (coordinated to only framework oxygens) Co^{2+} ions within zeolite Beta has been reported by Dedecek et al. [45]. These peaks arise from antisymmetric T-O-T skeletal vibrations that are perturbed (red-shifted) by the presence of bare Me^{2+} ions in exchange positions. Closely similar spectra have been reported for Co-Beta, Cu-SSZ-13, and Ni-FER catalysts and correlated with Me^{2+} ions occupying distinct ion-exchange sites that are populated sequentially with increasing metal loading [45,46]. For our Ni-H-Beta catalysts, a primary band at 945 cm^{-1} with a shoulder (or side band) at 970 cm^{-1} is observed. The intensity of these bands increases in proportion to Ni loading, as can be seen by comparing the Ni-H-Beta (H^+-1x) and Ni-H-Beta (H^+-4x) spectra (Figure 5A). The 945 cm^{-1} band is dominant for catalysts prepared from H-Beta irrespective of Ni loading. The 970 cm^{-1} band is more prominent in catalysts prepared from NH_4-Beta (Figure 5B); however, these catalysts also have higher Ni loadings. The T-O-T spectra strongly suggests that Ni^{2+} ions are located in two distinct exchange positions in zeolite Beta. The T-O-T frequencies, however, are 10–30 cm^{-1} higher than might be expected from previous reports on related Ni-zeolite catalysts, suggesting somewhat weaker interactions with framework oxygens.

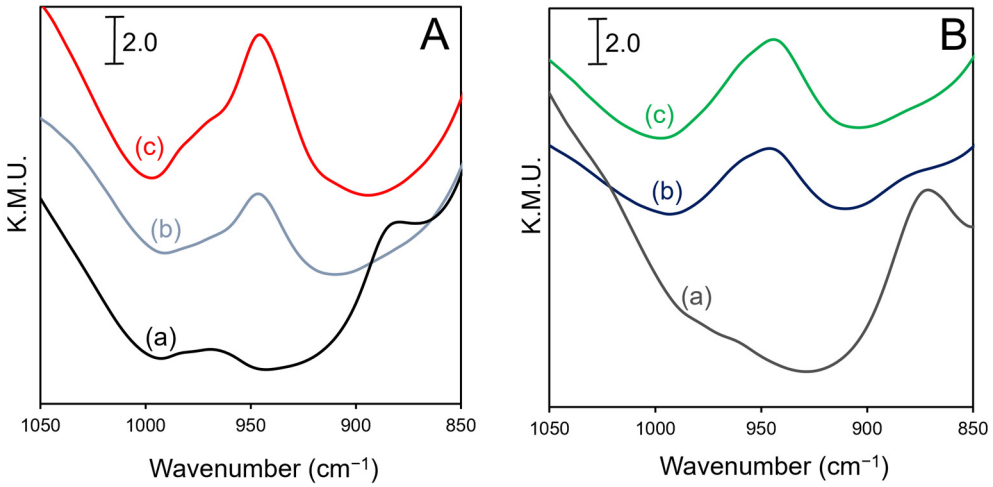

Figure 5. T-O-T DRIFT spectra of catalysts after in situ pretreatment at 350 °C. (**A**) (a) H-Beta, (b) Ni-H-Beta (H^+-1x), (c) Ni-H-Beta (H^+-4x); (**B**) (a) NH_4-Beta, (b) Ni-NH_4-Beta, (c) Ni-H-Beta (NH_4^+-4x).

The in situ DRIFT spectra of Ni carbonyl species following CO adsorption on the 4x-exchanged Ni-Beta catalysts at 20 °C are shown in Figure 6. The prominent CO-stretching (υ_{CO}) bands in the 2250–2200 cm^{-1} range are consistent with Ni^{2+}-CO species [27,47]. A

weak band at 2150 cm^{-1} assigned to CO adsorbed on NiO nanoparticles and very weak band at 2160 cm^{-1} are observed for Ni-H-Beta (H^+-4x) [48]. The v_{CO} bands of Ni^+-CO species typically appear at <2150 cm^{-1} and are not observed. A band at 2194 cm^{-1} ascribed in the literature to Ni^{2+} ions grafted to silanol nests is also absent. The v_{CO} bands for Ni-NH_4-Beta are significantly less intense than those for Ni-H-Beta (NH_4^+-4x); this is likely because of residual NH_3 coordinated to Ni^{2+} species in the former catalyst, as evidenced by TPDE. The Ni^{2+}-CO peak comprises components at 2211 cm^{-1} and 2203 cm^{-1}. The relative areas of the 2211 and 2203 cm^{-1} peaks, as determined by spectral deconvolution, are provided in Table S1. The 2211 cm^{-1} component constitutes approximately 70% of the total peak area for Ni-H-Beta (H^+-4x) and Ni-H-Beta (NH_4^+-4x). Similar bands are almost universally ascribed to CO interacting with bare Ni^{2+} ions in exchange positions. The 2203 cm^{-1} band, however, has several possible assignments. For example, Ni^{2+}-$(CO)_2$ species have been detected in Ni-H-Beta catalysts following CO adsorption at 100 K, but Ni^{2+} dicarbonyls are not expected to be stable at 20 °C [49]. Others have ascribed a similar band to monovalent $[NiOH]^+$ species or μ-oxo-Ni dimers ($[Ni\text{-}O\text{-}Ni]^{2+}$) [28,50]. Although the $[NiOH]^+$ assignment cannot be completely excluded in this work, we tentatively assign the 2203 cm^{-1} band to CO interacting with Ni^{2+} ions occupying an ion-exchange site distinct from that of the 2211 cm^{-1} band. Analogous assignments have been made for Ni-MOR [51]. The presence of bare Ni^{2+} ions in two different zeolite-Beta-exchange sites is also consistent with the T-O-T DRIFT spectra presented above.

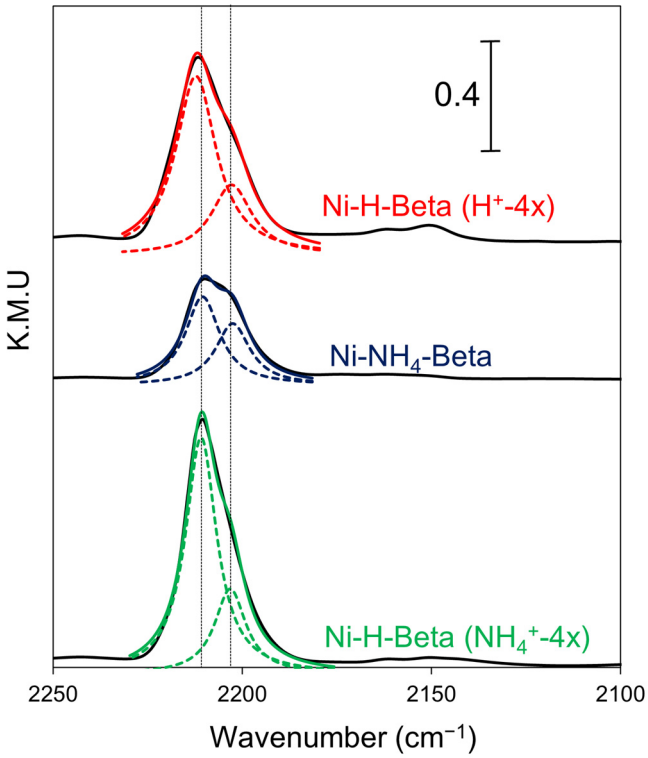

Figure 6. CO DRIFT spectra of catalysts after in situ pretreatment at 350 °C. Spectra measured after CO adsorption at 20 °C. Dashed curves are spectra deconvolutions.

The Lewis acidity of Me^{2+} ions in zeolites depends on the number of framework oxygens to which the ion is coordinated [27,47,50]. Thus, Ni^{2+} species with lower oxygen coordination numbers are expected to exhibit greater Lewis acidity, and Ni^{2+} ions occupying different ion-exchange sites in the Beta structure should display different CO-stretching frequencies. According to Dedecek et al., Me^{2+} ions in the γ-exchange site balance FAl present in opposite six-membered rings of the Beta hexagonal prisms in polymorphs A and B and are coordinated to six framework oxygens in a pseudo-octahedral geometry [45]. Alternatively, Me^{2+} ions in the β-exchange site charge-balance the FAl pairs present in six-

membered rings in the main channels of polymorphs A and B. The coordination geometry of Me^{2+} ions in the β site in trigonal planar; therefore, β-type Ni^{2+} ions should be more electrophilic than ions in the γ site and adsorbed CO should exhibit a higher stretching frequency. The α-exchange site consists of an elongated six-member ring resulting in fourfold coordination of an Me^{2+} ion that sits above the plane in a square pyramidal arrangement; however, this site only exists in polymorph C of zeolite Beta and is located within the hexagonal cages (prisms). If accessible, Ni^{2+} ions located in the α site of polymorph C should be of intermediate Lewis acidity. Commercial zeolite Beta typically comprises intergrowths of polymorphs A and B (in nearly equal proportions) with negligible polymorph C [36]. Thus, we assign the 2211 cm^{-1} υ_{CO} band to isolated Ni^{2+} ions in the β exchange positions and the 2203 cm^{-1} band to Ni^{2+} ions in γ positions. There should be equal numbers of each type of site available; however, Ni^{2+} ions in the γ position may be less able to coordinate CO owing to their lower accessibility.

2.4. NH_3 TPD

NH_3 TPD spectra of H-Beta and selected Ni-H-Beta catalysts are shown in Figure 7A. H-Beta exhibits a broad band at 350 °C (denoted HT1) that is assigned to BAS. The strong band centered at 220 °C (denoted LT1) is typically attributed to defect sites, such as coordinatively unsaturated framework Al ions [20]. The LT1 band also likely contains a component at 180 °C (depicted in the H-Beta TPD deconvolution, Figure S5) related to EFAl species. Difference spectra (obtained by subtracting the H-Beta spectrum from the others) are shown in Figure 7B. After Ni^{2+} exchange, a new band at 550 °C (denoted HT2) appears for Ni-H-Beta (H^+-4x) and Ni-H-Beta (NH_4^+-4x) that we assign to NH_3 adsorbed to strong Ni^{2+} Lewis acid sites (LAS) [52,53]. In addition, a negative HT1 peak in the TPD-difference profiles indicates a loss of BAS. Finally, the LT1 peak increases in intensity after Ni^{2+} exchange consistent with the intensity increase in the υ_{OH} EFAl band. The LT1 peak also appears to increase in proportion to the number of exchanges. The overall TCD signal intensity is higher for Ni-H-Beta (NH_4^+-4x) than for Ni-H-Beta (H^+-4x) in the >200 °C region, suggesting the presence of additional BAS. In comparison, Ni-H-Beta (H^+-1x) has lower overall signal intensity, and the HT2 peak is broad and centered around 570 °C.

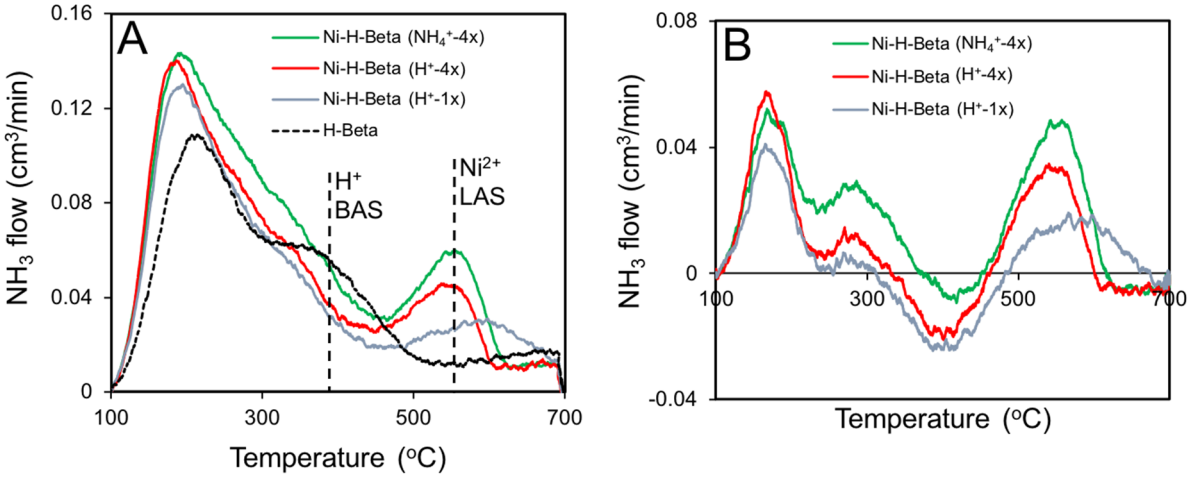

Figure 7. (**A**) NH_3 TPD spectra of H-Beta and Ni-H-Beta catalysts after in situ pretreatment at 500 °C and (**B**) TPD difference spectra (subtracting H-Beta reference).

The NH_3 TPD spectra of Ni-NH_4-Beta and Ni-H-Beta (NH_4^+-4x) were measured using online QMS to further elucidate the nature of the Ni^{2+} LAS. The TPD spectra of Ni-NH_4-Beta activated at 300 °C and 500 °C (Figure 8A,B) exhibit significant HT2 peaks at 550 °C that QMS reveals comprise H_2 and N_2. We infer that these peaks result from NH_3 decomposition analogous to that observed during TPDE. This observation is indicative of the strong Lewis acidity of Ni^{2+} ions occupying exchange positions in zeolite Beta. The NH_3/Ni molar ratio

(0.8) calculated from the QMS data suggests that if a single molecule binds to each Ni^{2+}, then NH_3 binds to ~80% of the potential sites (Table 1). The peak at 400 °C that coincides with the low-temperature TPDE peak (Figure 1B) is comprised primarily of H_2 and H_2O (see Figure S6). Concomitant NH_3 desorption evidences the presence of BAS in this catalyst. Tentatively, we assign the 400 °C NH_3 TPD peak to $[NiOH]^+/H^+$ species that charge-balance FAl pairs. The source of H_2 is not clear, but it does not appear to originate from NH_3 decomposition because N_2 desorption is not observed. Consistent with dehydration of $[NiOH]^+/H^+$ species, the 400 °C TPD peak does not survive activation at 500 °C, as shown in Figure 8B. Interestingly, this NH_3 TPD profile contains two HT2 peaks that both result from NH_3 decomposition suggesting the presence of two Ni^{2+} sites. The NH_3/Ni atomic ratio (0.9) suggests that NH_3 binds to ~90% of the potential sites. Finally, the NH_3 TPD spectrum of Ni-H-Beta (NH_4^+-4x) (Figure 8C) contains a sharp HT2 band at 570 °C that results primarily from concomitant H_2 and N_2 evolution. The NH_3/Ni atomic ratio (0.44) suggests that NH_3 binds to only approximately half of the potential sites. To our knowledge, this is the first report of H_2 and N_2 generation from NH_3 adsorbed on Ni-H-Beta catalysts; Ni/ZSM-5 has been previously reported to be an NH_3 decomposition catalyst [54].

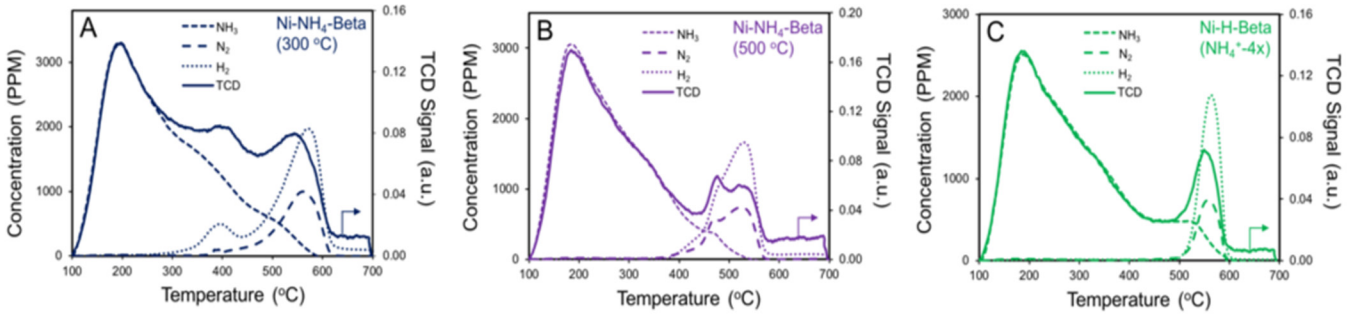

Figure 8. NH_3 TPD using online QMS. (**A**) Ni-NH_4-Beta pretreated in situ at 300 °C, (**B**) Ni-NH_4-Beta pretreated in situ at 500 °C, and (**C**) Ni-H-Beta (NH_4^+-4x) pretreated in situ at 500 °C.

The NH_3 TPD spectrum of Ni-H-Beta (H^+-3x) (Figure 9A) is qualitatively similar to that of Ni-H-Beta (H^+-4x) except the HT2 band appears at somewhat higher temperature (~600 °C). The QMS data confirm that NH_3 decomposition occurs with a NH_3/Ni ratio of ~0.43 in excellent agreement with the above result for Ni-H-Beta (NH_4^+-4x), and both of these catalysts contain primarily Ni^{2+} ions in exchange sites. In contrast, the lower loading catalyst Ni-H-Beta (H^+-1x) (Figure 9B) exhibits a NH_3 desorption in a broad band centered around 580 °C with negligible H_2 and N_2 generation. This loading effect remains to be elucidated, but the NH_3 decomposition reaction ($2NH_3 \rightarrow N_2 + 3H_2$) may require two nearby Ni^{2+} ions. The H/N molar ratio for all samples exhibiting H_2 and N_2 desorption was approximately 2 (Table 1). A ratio of 3 would be expected from the stoichiometry; this suggests that Ni^{2+} species may be reduced, consuming the additional hydrogen.

2.5. Ethylene Oligomerization

The Ni-H-Beta catalysts were active for EO at 225 °C and 11 bar (WHSV = 3 h^{-1}) after in situ pretreatment at 300 °C in flowing N_2 (Figure 10A). In comparison, H-Beta displayed <5% conversion under these reaction conditions. Interestingly, Ni-NH_4-Beta displayed comparable activity to Ni-H-Beta (NH_4^+-4x), suggesting that $[NiOH]^+$ species can serve as precursors of the Cossee–Arlman-active centers. The calcined catalyst containing primarily bare Ni^{2+} in exchange positions was only slightly more active. DFT calculations by Brogaard et al. [16] revealed that pathways to the Cossee–Arlman-active center from bare Ni^{2+} and $[NiOH]^+$ have similar activation energies. Because both catalysts contain BAS, the difference in activity probably results from poisoning of Ni^{2+} sites by residual adsorbed NH_3 molecules in Ni-NH_4-Beta. Steady-state EO conversion is expected to increase with Ni loading; however, the effect was smaller than expected for Ni-H-Beta (H^+-4x) relative to Ni-H-Beta (H^+-1x). After activation at 300 °C, Ni-H-Beta (H^+-4x) contains a mixture

of $[NiOH]^+$ and bare Ni^{2+} species with small amounts of presumably inactive NiO [15]. If a significant fraction of Ni^{2+} ions in Ni-H-Beta (H^+-4x) are in γ sites, as suggested by T-O-T and CO DRIFTS, they may be unable to coordinate ethylene molecules owing to their inaccessibility and pseudo-octahedral oxygen coordination.

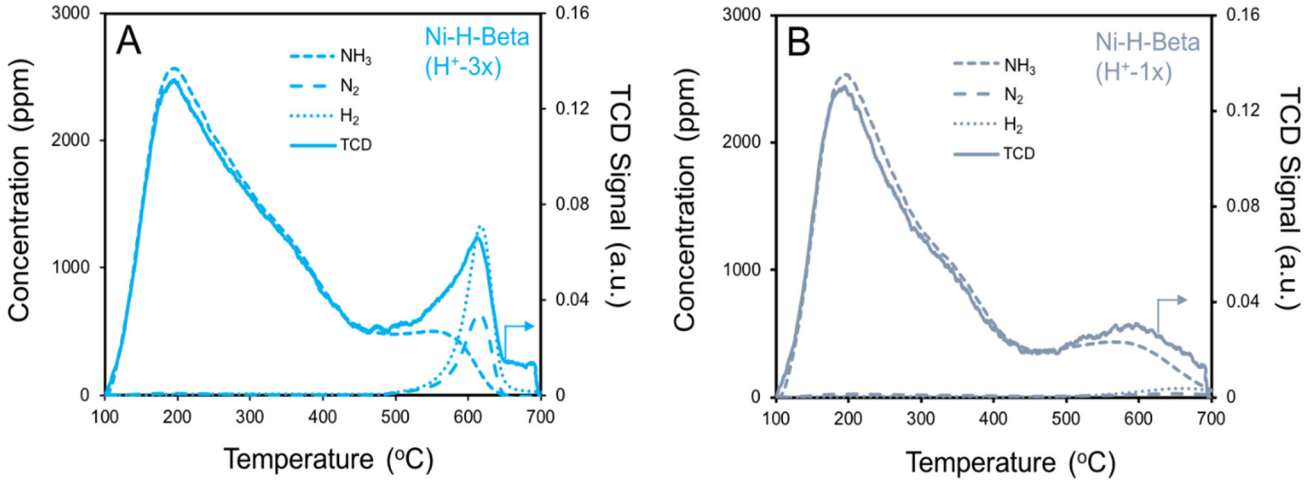

Figure 9. NH_3 TPD with online QMS after in situ pretreatment at 500 °C. (**A**) Ni-H-Beta (H^+-3x) and (**B**) Ni-H-Beta (H^+-1x).

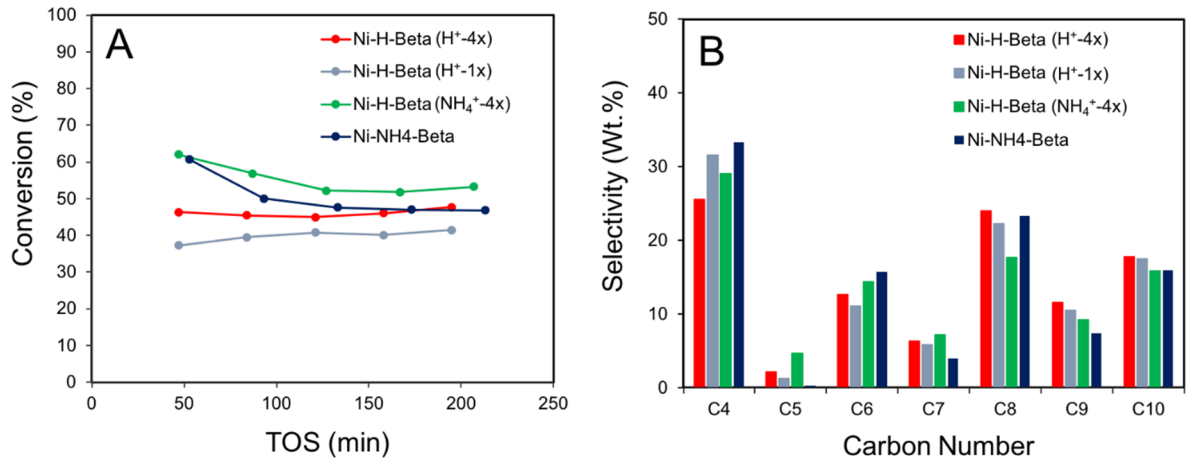

Figure 10. EO over Ni-H-Beta catalysts after in situ pretreatment at 300 °C in N_2. T = 225 °C, P = 11 bar, WHSV = 3 h^{-1}: (**A**) Conversion with time on stream (TOS) and (**B**) steady-state oligomer distribution.

The Ni-H-Beta catalysts exhibited only ~30% selectivity to butenes and high selectivity to C6-C10 oligomers, thus deviating markedly from a Schulz–Flory distribution (Figure 10B). Moreover, selectivity to octenes (~20%) was higher than hexenes (~15%) selectivity. These deviations from a Schulz–Flory distribution can be attributed co-oligomerization involving BAS that dimerize butenes to octenes and also crack even-numbered oligomers to odd-numbered products [55,56]. The Ni-H-Beta (NH_4^+-4x) catalyst exhibited slightly lower C8+ oligomer selectivity compared with Ni-H-Beta (H^+-4x). We suggest this to be the result of a higher BAS/Ni^{2+} ratio in the case of the latter. Selectivity to *cis*- and *trans*-C4 remains almost constant once the reaction reaches steady state, but *i*-C4 selectivity (a marker of BAS activity) declines to almost zero after <1 h (see Figure S7). This result suggests that the double-bond isomerization of 1-butene to *cis*- and *trans*-butene is performed primarily by Ni^{2+} sites. Others have claimed double-bond isomerization to be indicative of BAS activity [8,57], but this pathway has recently been reported in BAS-free Ni-Beta catalysts by Joshi et al. [17].

3. Materials and Methods

3.1. Catalyst Preparation

NH_4-Beta (SiO_2/Al_2O_3 = 25, CP814E, Lot#2200-42) was obtained from Zeolyst International (Conshohocken, PA, USA). The as-received NH_4-Beta was calcined in flowing air at 600 °C for 4 h to yield H-Beta. Ni-H-Beta (H^+-*n*x) (*n* = 1–4) catalysts were prepared by exchanging H-Beta *n* times at 70 °C for 4 h with 0.1 M $Ni(NO_3)_2{\cdot}6H_2O$ (Sigma Aldrich (St. Louis, MO, USA)) (10 cm^3/g zeolite) [13]. After each exchange, the solid was washed with deionized water, dried overnight at 120 °C, and ground to a powder. After the final exchange, the resultant solid was calcined at 550 °C in flowing air for 4 h. Ni-NH_4-Beta was prepared by quadruple exchange of NH_4-Beta with a 0.1 M $Ni(NO_3)_2.6H_2O$ solution at 70 °C for 4 h. The solid was washed, filtered, and dried, as described above. Calcination of Ni-NH_4-Beta in flowing air at 550 °C for 4 h yielded Ni-H-Beta (NH_4^+-4x). Ni loadings were determined by Galbraith Laboratories (Knoxville, TN, USA) using inductively coupled plasma–optical emission spectrometry (ICP-OES). The Si/Al ratio of H-Beta measured by ICP-OES (11.8) agrees reasonably well with the vendor specification.

3.2. Catalyst Characterization

X-ray diffractograms were measured using a Rigaku (Woodlands, TX, USA) SmartLab instrument equipped with a Cu Kα source (λ = 0.1542 nm). N_2 adsorption–desorption isotherms at 77 K were measured using a Micromeritics (Norcross, GA, USA) ASAP 2020c instrument. Total pore volumes were evaluated at P/P_0 = 0.99, specific surface areas were calculated using the Brunauer–Emmett–Teller (BET) method (P/P_0 = 0.02–0.2 range), and mesopore–size distributions were computed using the Barrett–Joyner–Haleda (BJH) method. H_2 TPR and NH_3 TPD measurements were performed using a Micromeritics AutoChem II 2920 equipped with a calibrated thermal conductivity detector (TCD) and Pfeiffer (Nashua, NH, USA) Prisma quadrupole mass spectrometer (QMS) with a capillary inlet system. An isopropanol liquid N_2 trap was located downstream of the sample to trap condensable species. In a typical TPR experiment, a 150 mg sample was pretreated in situ by heating to 300 (or 500) °C at 10 °C/min in flowing He (50 sccm) and holding for 60 min. After being cooled to ambient temperature, gas flow was switched to 50 sccm of 5% H_2/Ar (Airgas, RTP, NC, USA) and held at 0 °C (or 20 °C) for 45 min to establish a stable TCD baseline. Then, the sample temperature was ramped to 800 °C at 10 °C/min. For NH_3 TPD experiments, a 100 mg sample was pretreated in situ by heating to 500 °C at 10 °C/min in flowing He (50 sccm) and holding for 30 min. After cooling to 100 °C, the flow was switched to 1% NH_3/He (Arc3 Gases, RTP, NC, USA), and the catalyst was purged at 50 sccm for 20 min. Then, the flow was switched back to He, and the catalyst was purged for 60 min to remove physisorbed NH_3. Subsequently, the temperature was ramped to 700 °C at 10 °C/min in flowing He and desorbed products were monitored by calibrated TCD (NH_3) and online QMS for H_2 (*m*/*z* = 2), NH_3 (*m*/*z* = 17), and N_2 (*m*/*z* = 28).

The DRIFT spectra of the catalysts before and after CO adsorption at 20 °C were recorded using a Bruker (Billerica, MA, USA) Vertex 70 FTIR spectrometer equipped with an MCT detector, a Harrick (Pleasantville, NY, USA) Praying Mantis accessory, and in situ reaction cell. Samples (50 mg) were pretreated in situ by heating to 350 °C at 10 °C/min in flowing He (50 sccm) and holding for 60 min. After cooling to 20 °C, a baseline spectrum was recorded at 2 cm^{-1} resolution using 128 scans. Subsequently, a Valco (Houston, TX, USA) injection valve was used to pulse 99.999% CO (Research grade, Airgas) into the He stream, and additional spectra were recorded until no change in the ν(CO) region was observed.

3.3. Ethylene Oligomerization

EO testing was conducted using a 0.5 in. ID 316 stainless-steel fixed-bed flow reactor heated by a Linberg Blue-M (Waltham, MA, USA) furnace. Gases were metered by mass flow controllers. In a typical run, 0.50 g of catalyst was supported in the reactor by quartz wool plugs, and a Type K thermocouple was inserted into the bed for temperature

measurement. Pressure was controlled by a Tescom (Elk River, MN, USA) back-pressure regulator. Before each run, the reactor was secured into position and pressurized to 11 bar with N_2 and checked for leaks. Then, the reactor was depressurized, and the catalyst was activated by heating to 300 °C in 100 sccm of flowing N_2 and held for 1 h to ensure the sample was free of physisorbed H_2O. The catalyst temperature was then reduced to 225 °C and the reactor was pressurized to 11 bar with ethylene (99.999% purity, Airgas (Radnor, PA, USA)). Using 22 mL/min (22 °C, 1 atm) of ethylene gave a weight hourly space velocity of 3 h^{-1}. All lines downstream of the reactor were wrapped with heating tape and held at 150 °C to prevent the condensation of reaction products. A Valco 6-port sampling valve was positioned to automatically sample the reactor effluent for analysis using a Shimadzu (Columbia, MD, USA) GC-2010 equipped with a Restek (Bellefonte, PA, USA) Rt-Q-Bond PLOT column and a flame ionization detector. Oligomer products were identified in the chromatograms using the retention times of known standards (Millipore Sigma (Burlington, MA, USA) SCOTTY Gases). Ethylene conversion was calculated by dividing its peak area by the total GC area and subtracting the quotient from unity. Product selectivity was calculated by dividing the specific GC peak area by the sum of the peak areas of all products. The GC column was able to resolve butene into its 4 isomers (1, iso, cis and trans); however, all higher oligomer products presented grouped peaks which could not be further resolved.

4. Conclusions

The Ni^{2+} exchange capacity of H-Beta is approximately 20% lower than NH_4-Beta. This difference can be explained by hydrolysis of FAl sites in H-Beta forming framework-associated Al^{3+} species and lowering the overall exchange capacity. Moreover, exchange of NH_4-Beta with aqueous $Ni(NO_3)_2$ results predominantly in monovalent $[NiOH]^+$ and H^+ species charge-balancing FAl sites. Calcination of Ni-NH_4-Beta resulted in a catalyst containing bare Ni^{2+} ions and H^+ in exchange positions. In contrast, calcined Ni-H-Beta prepared from H-Beta contains a mixture of bare Ni^{2+} ions: $[NiOH]^+$ and NiO species. NiO was detected as a minority species in all Ni-H-Beta catalysts. The $[NiOH]^+$ species were dehydrated by in situ pretreatment at 500 °C, resulting in bare Ni^{2+} ions coordinated only to framework oxygen atoms. Strong interaction of Ni^{2+} ions with the Beta framework is evidenced by a perturbed antisymmetric T-O-T skeletal vibration at 945 cm^{-1}. CO DRIFTS evidenced two distinct Ni^{2+}-CO species that we infer are located in the β-exchange site (majority) and γ-exchange site. Ni-H-Beta catalysts prepared from H-Beta and NH_4-Beta exhibited comparable EO activity at 225 °C and 11 bar indicating that both bare Ni^{2+} ions and $[NiOH]^+$ species may serve as precursors of Cossee–Arlman-active sites. Thus, it is unnecessary to begin with H-Beta to prepare active Ni-H-Beta catalysts by ion exchange, and catalysts prepared by Ni^{2+} exchange of NH_4-Beta have higher activity owing to their higher Ni loadings. The olefin product distributions are non-Schulz–Flory, consistent with co-oligomerization involving BAS irrespective of the parent cation (H^+ or NH_4^+).

Supplementary Materials: The following Supplementary Materials can be downloaded at: https://www.mdpi.com/article/10.3390/catal12080824/s1, Figure S1: X-ray diffraction (XRD) powder patterns of the parent zeolites and selected Ni-H-Beta (H^+-*n*x) catalysts; Figure S2: Pore size distributions of parent zeolites and Ni-H-Beta catalysts calculated from 77K N_2 desorption data using the BJH method; Figure S3: H2 TPR of Ni-NH_4-Beta following pretreatment at 300 °C in He monitored by TCD and QMS (secondary axis). H_2 consumption (TCD) and QMS signals of CH_4 (m/z = 16), NH_3 (m/z = 17), and N_2 (m/z = 28) are shown; Figure S4: *v*(OH) DRIFT spectra of H-Beta produced by calcination of NH_4-Beta at 500 and 600 °C in flowing air. Samples were pretreated in situ at 350 °C in the DRIFTS cell; Figure S5: NH_3 TPD of H-Beta following pretreatment at 500 °C in He. Peak deconvolutions performed on ORIGIN software; Figure S6: NH_3 TPD of Ni-NH_4-Beta following pretreatment at 300 °C in He monitored by on-line QMS; Figure S7: EO butene selectivities for Ni-Beta catalysts following activation at 300 °C in N_2. T = 225 °C, P = 11 bar, WHSV = 3 h^{-1}; Table S1: CO DRIFTS peak proportions for Ni-Beta catalysts. Deconvolutions performed on commercial ORIGIN software.

Author Contributions: Conceptualization, H.H.L.; Formal analysis, J.M.; Funding acquisition, H.H.L.; Investigation, J.M.; Methodology, J.M.; Supervision, H.H.L. All authors have read and agreed to the published version of the manuscript.

Funding: This work was supported by the AIChE/DOE RAPID Institute (DE-EE0007888-05-6).

Data Availability Statement: All pertinent data are provided in the manuscript or Supplementary Materials.

Acknowledgments: The authors acknowledge Kyle Vogt-Lowell for his assistance with the XRD measurements.

Conflicts of Interest: The authors declare no conflict of interest.

References

1. Weyant, C.; Shepson, P.; Subramanian, R.; Cambaliza, M.; Heimburger, A.; McCabe, D.; Baum, E.; Stirm, B.; Bond, T. Black carbon emissions from associated natural gas flaring. *Environ. Sci. Technol.* **2016**, *50*, 2075–2081. [CrossRef]
2. Feijoo, F.; Iyer, G.; Avraam, C.; Siddiqui, S.; Clarke, L.; Sankaranarayanan, S.; Binsted, M.; Patel, P.; Prates, N.; Torres-Alfaro, E.; et al. The future of natural gas infrastructure development in the United States. *Appl. Energy* **2018**, *228*, 149–166. [CrossRef]
3. Neal, L.; Haribal, V.; McCaig, J.; Lamb, H.; Li, F. Modular-scale ethane to liquids via chemical looping oxidative dehydrogenation: Redox catalyst performance and process analysis. *J. Adv. Manuf. Process.* **2019**, *1*, e10015. [CrossRef]
4. Novotný, P.; Yusuf, S.; Li, F.; Lamb, H. Oxidative dehydrogenation of ethane using MoO_3/Fe_2O_3 catalysts in a cyclic redox mode. *Catal. Today* **2018**, *317*, 50–55. [CrossRef]
5. Lutz, E. Shell higher olefins process. *J. Chem. Educ.* **1986**, *63*, 202. [CrossRef]
6. Small, B.; Brookhart, M. Iron-based catalysts with exceptionally high activities and selectivities for oligomerization of ethylene to linear α-Olefins. *J. Am. Chem. Soc.* **1998**, *120*, 7143–7144. [CrossRef]
7. Lallemand, M.; Finiels, A.; Fajula, F.; Hulea, V. Catalytic oligomerization of ethylene over Ni-containing dealuminated Y zeolites. *Appl. Catal. A Gen.* **2006**, *301*, 196–201. [CrossRef]
8. Lallemand, M.; Rusu, O.; Dumitriu, E.; Finiels, A.; Fajula, F.; Hulea, V. NiMCM-36 and NiMCM-22 catalysts for the ethylene oligomerization: Effect of zeolite texture and nickel cations/acid sites ratio. *Appl. Catal. A Gen.* **2008**, *338*, 37–43. [CrossRef]
9. Heydenrych, M.; Nicolaides, C.; Scurrell, M. Oligomerization of ethene in a slurry reactor using a nickel(II)-exchanged silica–alumina catalyst. *J. Catal.* **2001**, *197*, 49–57. [CrossRef]
10. Andrei, R.; Popa, M.; Fajula, F.; Hulea, V. Heterogeneous oligomerization of ethylene over highly active and stable Ni-AlSBA-15 mesoporous catalysts. *J. Catal.* **2015**, *323*, 76–84. [CrossRef]
11. Lee, M.; Yoon, J.; Kim, Y.; Yoon, J.; Chae, H.; Han, Y.; Hwang, D. Ni/SIRAL-30 as a heterogeneous catalyst for ethylene oligomerization. *Appl. Catal. A Gen.* **2018**, *562*, 87–93. [CrossRef]
12. Lehmann, T.; Wolff, T.; Zahn, V.; Veit, P.; Hamel, C.; Seidel-Morgenstern, A. Preparation of Ni-MCM-41 by equilibrium adsorption—Catalytic evaluation for the direct conversion of ethene to propene. *Catal. Commun.* **2011**, *12*, 368–374. [CrossRef]
13. Martínez, A.; Arribas, M.; Concepción, P.; Moussa, S. New Bifunctional Ni–H-Beta Catalysts for the heterogeneous oligomerization of ethylene. *Appl. Catal. A Gen.* **2013**, *467*, 509–518.
14. Jan, O.; Song, K.; Dichiara, A.; Resende, F. Ethylene oligomerization over Ni–Hβ heterogeneous catalysts. *Ind. Eng. Chem. Res* **2018**, *57*, 10241–10250. [CrossRef]
15. Henry, R.; Komurcu, M.; Ganjkhanlou, Y.; Brogaard, R.; Lu, L.; Jens, K.; Berlier, G.; Olsbye, U. Ethene oligomerization on nickel microporous and mesoporous-supported catalysts: Investigation of the active sites. *Catal. Today* **2018**, *299*, 154–163. [CrossRef]
16. Brogaard, R.; Olsbye, U. Ethene oligomerization in Ni-containing zeolites: Theoretical discrimination of reaction mechanisms. *ACS Catal.* **2016**, *6*, 1205–1214. [CrossRef]
17. Joshi, R.; Zhang, G.; Miller, J.; Gounder, R. Evidence for the coordination–insertion mechanism of ethene dimerization at nickel cations exchanged onto beta molecular sieves. *ACS Catal.* **2018**, *8*, 11407–11422. [CrossRef]
18. Moussa, S.; Arribas, M.; Concepcion, P.; Martinez, A. Heterogeneous oligomerization of ethylene to liquids on bifunctional Ni-Based Catalysts: The influence of support properties on nickel speciation and catalytic performance. *Catal. Today* **2016**, *277*, 78–88. [CrossRef]
19. Seufitelli, G.; Park, J.; Tran, P.; Dichiara, A.; Resende, F.; Gustafson, R. Kinetics of ethylene oligomerization over Ni-H-beta catalysts. *J. Catal.* **2021**, *401*, 40–53.
20. Lónyi, F.; Valyon, J. A TPD and IR study of the surface species formed from ammonia on zeolite H-ZSM-5, H-Mordenite and H-Beta. *Thermochim. Acta* **2001**, *373*, 53–57. [CrossRef]
21. Rice, M.J.; Chakraborty, A.K.; Bell, A.T. Site availability and competitive siting of divalent metal cations in ZSM-5. *J. Catal.* **2000**, *194*, 278–285. [CrossRef]
22. Kunkeler, P.; Zuurdeeg, B.; van der Waal, J.; van Bokhoven, J.; Koningsberger, D.; van Bekkum, H. zeolite Beta: The relationship between calcination procedure, aluminum configuration, and Lewis acidity. *J. Catal.* **1998**, *180*, 234–244. [CrossRef]
23. Wouters, B.H.; Chen, T.H.; Grobet, P.J. Reversible tetrahedral-octahedral framework aluminum transformation in zeolite Y. *J. Am. Chem. Soc.* **1998**, *120*, 11419–11425. [CrossRef]

24. Bourgeat-Lami, E.; Massiani, P.; Di Renzo, F.; Espiau, P.; Fajula, F.; Des Courieres, T. Study of the state of aluminium in zeolite Beta. *Appl. Catal.* **1991**, *72*, 139–152. [CrossRef]
25. Abraham, A.; Lee, S.; Shin, C.; Bong Hong, S.; Prins, R.; van Bokhoven, J. Influence Of framework silicon to aluminium ratio on aluminium coordination and distribution in zeolite beta investigated by ^{27}Al MAS and ^{27}Al MQ MAS NMR. *Phys. Chem. Chem. Phys.* **2004**, *6*, 3031. [CrossRef]
26. Ravi, M.; Sushkevich, V.L.; van Bokhoven, J.A. Towards a better understanding of Lewis acidic aluminium in zeolites. *Nat. Mater.* **2020**, *19*, 1047–1056. [CrossRef] [PubMed]
27. Penkova, A.; Dzwigaj, S.; Kefirov, R.; Hadjiivanov, K.; Che, M. Effect of the preparation method on the state of nickel ions in BEA zeolites. A study by fourier transform infrared spectroscopy of adsorbed CO and NO, temperature-programmed reduction, and X-ray diffraction. *J. Phys. Chem. C* **2007**, *111*, 8623–8631. [CrossRef]
28. Kyounghwan, L.; Hong, S.B. Ethene dimerization over Ni-beta catalysts prepared by solid-state ion exchange. *Appl. Catal. A Gen.* **2021**, *615*, 118059.
29. Suzuki, M.; Tsutsumi, K.; Takahashi, H.; Saito, Y. Study on reducibility of nickel ions in zeolite Y. *Zeolites* **1989**, *9*, 98–103. [CrossRef]
30. Stoyanova, M.; Bentrup, U.; Atia, H.; Kondratenko, E.; Linke, D.; Rodemerck, U. The role of speciation Of Ni^{2+} and its interaction with the support for selectivity and stability in the conversion of ethylene to propene. *Catal. Sci. Technol.* **2019**, *9*, 3137–3148.
31. Mihályi, R.; Lónyi, F.; Beyer, H.; Szegedi, Á.; Kollár, M.; Pál-Borbély, G.; Valyon, J. N-Heptane hydroconversion over nickel-loaded aluminum- and/or boron-containing BEA zeolites prepared by recrystallization of magadiite varieties. *J. Mol. Catal. A Chem.* **2013**, *367*, 77–88. [CrossRef]
32. Ward, J.W. The nature of active sites on zeolites III. The alkali and alkaline earth ion-exchanged forms. *J. Catal.* **1968**, *10*, 34–46. [CrossRef]
33. Jacobs, P.A. Metal clusters and zeolites. In *Metal Clusters in Catalysis*; Gates, B.C., Guczi, L., Knozinger, H., Eds.; Elsevier: Amsterdam, the Netherlands, 1986; pp. 357–414.
34. Hoang, D.; Berndt, H.; Miessner, H.; Schreier, E.; Völter, J.; Lieske, H. Nickel modified H-ZSM-5 catalysts. *Appl. Catal. A Gen.* **1994**, *114*, 295–311. [CrossRef]
35. Kiricsi, I.; Flego, C.; Pazzuconi, G.; Parker, W.; Millini, R.; Perego, C.; Bellussi, G. Progress toward understanding zeolite beta acidity: An IR and ^{27}Al NMR spectroscopic study. *J. Phys. Chem.* **1994**, *98*, 4627–4634. [CrossRef]
36. Newsam, J.M.; Treacy, M.M.J.; Koetsier, W.T.; De Gruyter, C.B. Structural characterization of zeolite beta. *Proc. R. Soc. A.* **1988**, *420*, 375–405.
37. Marques, J.; Gener, I.; Ayrault, P.; Bordado, J.; Lopes, J.; Ramôa Ribeiro, F.; Guisnet, M. Infrared spectroscopic study of the acid properties of dealuminated BEA zeolites. *Microporous Mesoporous Mater.* **2003**, *60*, 251–262. [CrossRef]
38. Shannon, R.D.; Gardner, K.H.; Staley, R.H. The nature of the nonframework aluminum species formed during the dehydroxylation of H-Y. *J. Phys. Chem.* **1985**, *89*, 4778–4788. [CrossRef]
39. Zholobenko, V.; Kustov, L.; Kazansky, V.; Loeffler, E.; Lohser, U.; Peuker, C.; Oehlmann, G. On The possible nature of sites responsible for the enhancement of cracking activity of HZSM-5 zeolites dealuminated under mild steaming conditions. *Zeolites* **1990**, *10*, 304–306. [CrossRef]
40. Jacobs, P.A. Evidence for the nature of true Lewis sites in faujasite-type zeolites. *J. Phys. Chem.* **1979**, *83*, 1174. [CrossRef]
41. Vimont, A.; Thibault-Starzyk, F.; Lavalley, J.C. Infrared spectroscopic study of the acidiobasic properties of zeolite beta. *J. Phys. Chem.* **2000**, *104*, 286–291. [CrossRef]
42. Sobalík, Z.; Dêdecek, J.; Kaucký, D.; Wichterlová, B.; Drozdová, L.; Prins, R.J. Structure, distribution, and properties of Co ions in ferrierite revealed by FTIR, UV–Vis, and EXAFS. *J. Catal.* **2000**, *194*, 330–342. [CrossRef]
43. Borfecchia, E.; Lomachenko, K.; Giordanino, F.; Falsig, H.; Beato, P.; Soldatov, A.; Bordiga, S.; Lamberti, C. Revisiting the nature of Cu sites in the activated Cu-SSZ-13 catalyst for SCR reaction. *Chem. Sci.* **2015**, *6*, 548–563. [CrossRef] [PubMed]
44. Hall, D.; Lockwood, D.; Poirier, S.; Bock, C.; MacDougall, B. Raman and infrared spectroscopy of A and B phases of thin nickel hydroxide films electrochemically formed on Nickel. *J. Phys. Chem. A* **2012**, *116*, 6771–6784. [CrossRef] [PubMed]
45. Dedecek, J. Siting and distribution of the Co ions in zeolite beta: A UV–Vis–NIR and FTIR study. *J. Catal.* **2002**, *211*, 198–207. [CrossRef]
46. Hun Kwak, J.; Zhu, H.; Lee, J.; Peden, C.; Szanyi, J. Two different cationic positions in Cu-SSZ-13. *Chem. Commun.* **2012**, *48*, 4758. [CrossRef] [PubMed]
47. Hadjiivanov, K.; Knözinger, H.; Mihaylov, M. FTIR Study of CO adsorption on Ni−ZSM-5. *J. Phys. Chem. B* **2002**, *106*, 2618–2624. [CrossRef]
48. Mihaylov, M.; Hadjiivanov, K. FTIR study of CO and NO adsorption and coadsorption on Ni-ZSM-5 and Ni/SiO_2. *Langmuir* **2002**, *18*, 4376–4383. [CrossRef]
49. Hadjivanov, K.; Vayssilov, G. Characterization of oxide surfaces and zeolites by carbon monoxide as an IR probe molecule. *Adv. Catal.* **2002**, *47*, 307–511. [CrossRef]
50. Góra-Marek, K.; Glanowska, A.; Datka, J. Quantitative IR studies of the concentration of different nickel sites in NiZSM-5 zeolites. *Microporous Mesoporous Mater.* **2012**, *158*, 162–169. [CrossRef]
51. Campa, M.; Pietrogiacomi, D.; Occhiuzzi, M. The simultaneous selective catalytic reduction of N_2O and NO_X with CH_4 on Co- and Ni-exchanged mordenite. *Appl. Catal. B* **2015**, *168–169*, 293–302. [CrossRef]

52. Yan, P.; Li, M.; Kennedy, E.; Adesina, A.; Zhao, G.; Setiawan, A.; Stockenhuber, M. The role of acid and metal sites in hydrodeoxygenation of guaiacol over Ni/Beta catalysts. *Catal. Sci. Technol.* **2020**, *10*, 810–825. [CrossRef]
53. Lin, T.; Meng, X.; Shi, L. Ni-exchanged Y-Zeolite: An efficient heterogeneous catalyst for acetylene hydrocarboxylation. *Appl. Catal. A Gen.* **2014**, *485*, 163–171. [CrossRef]
54. Hu, Z.; Weng, C.; Chen, C.; Yuan, Z. Catalytic decomposition of ammonia to CO_X-free hydrogen over Ni/ZSM-5 catalysts: A comparative study of the preparation methods. *Appl. Catal. A Gen.* **2018**, *562*, 49–57. [CrossRef]
55. Toch, K.; Thybaut, J.; Arribas, M.; Martínez, A.; Marin, G. Steering linear 1-Alkene, propene or gasoline yields in ethene oligomerization via the interplay between nickel and acid sites. *Chem. Eng. Sci.* **2017**, *173*, 49–59. [CrossRef]
56. Lallemand, M.; Finiels, A.; Fajula, F.; Hulea, V. Nature of The active sites in ethylene oligomerization catalyzed by Ni-containing molecular sieves: Chemical and IR spectral investigation. *J. Phys. Chem C* **2009**, *113*, 20360–20364. [CrossRef]
57. Hulea, V.; Fajula, F. Ni-exchanged AlMCM-41: An efficient bifunctional catalyst for ethylene oligomerization. *J. Catal.* **2004**, *225*, 213–222. [CrossRef]